Journal of Visualized Experiments

Preparation of silver-palladium alloyed nanoparticles for plasmonic catalysis under visible-light illumination

--Manuscript Draft--

Article Type:	Invited Methods Article - JoVE Produced Video
Manuscript Number:	JoVE61712R1
Full Title:	Preparation of silver-palladium alloyed nanoparticles for plasmonic catalysis under visible-light illumination
Section/Category:	JoVE Chemistry
Keywords:	Plasmonic catalysis; localized surface plasmon resonance; bimetallic nanoparticles; alloyed nanoparticles; silver; palladium; photocatalysis
Corresponding Author:	Pedro Camargo FINLAND
Corresponding Author's Institution:	
Corresponding Author E-Mail:	pedro.camargo@helsinki.fi
Order of Authors:	Erandi Peiris
	Sebastien Hanauer
	Kjell Knapas
	Pedro Camargo
Additional Information:	
Question	**Response**
Please indicate whether this article will be Standard Access or Open Access.	Standard Access (US$2,400)
Please indicate the **city, state/province, and country** where this article will be **filmed**. Please do not use abbreviations.	Helsinki, Finland

TITLE:

Preparation of Silver-Palladium Alloyed Nanoparticles for Plasmonic Catalysis Under Visible-Light Illumination

AUTHORS AND AFFILIATIONS:

Erandi Peiris[1], Sébastien Hanauer[1], Kjell Knapas[1], Pedro H. C. Camargo[1]

[1]Department of Chemistry, University of Helsinki, A.I. Virtasen aukio 1, Helsinki, Finland

Corresponding author:
Pedro H. C. Camargo (pedro.camargo@helsinki.fi)

Email addresses of co-authors:
Erandi Peiris (erandi.prangige@helsinki.fi)
Sébastien Hanauer (sebastien.hanauer@helsinki.fi)
Kjell Knapas (kjell.knapas@helsinki.fi)

KEYWORDS:

plasmonic catalysis, localized surface plasmon resonance, bimetallic nanoparticles, alloyed nanoparticles, silver, palladium, photocatalysis

SUMMARY:

Presented here is a protocol for the synthesis of silver-palladium (Ag-Pd) alloy nanoparticles (NPs) supported on ZrO_2 (Ag-Pd/ZrO_2). This system allows for harvesting energy from visible light irradiation to accelerate and control molecular transformations. This is illustrated by nitrobenzene reduction under light irradiation catalyzed by Ag-Pd/ZrO_2 NPs.

ABSTRACT:

Localized surface plasmon resonance (LSPR) in plasmonic nanoparticles (NPs) can accelerate and control the selectivity of a variety of molecular transformations. This opens possibilities for the use of visible or near-IR light as a sustainable input to drive and control reactions when plasmonic nanoparticles supporting LSPR excitation in these ranges are employed as catalysts. Unfortunately, this is not the case for several catalytic metals such as palladium (Pd). One strategy to overcome this limitation is to employ bimetallic NPs containing plasmonic and catalytic metals. In this case, the LSPR excitation in the plasmonic metal can contribute to accelerate and control transformations driven by the catalytic component. The method reported herein focuses on the synthesis of bimetallic silver-palladium (Ag-Pd) NPs supported on ZrO_2 (Ag-Pd/ZrO_2) that acts as a plasmonic-catalytic system. The NPs were prepared by co-impregnation of corresponding metal precursors on the ZrO_2 support followed by simultaneous reduction leading to the formation of bimetallic NPs directly on the ZrO_2 support. The Ag-Pd/ZrO_2 NPs were then used as plasmonic catalysts for the reduction of nitrobenzene under 425 nm illumination by LED lamps. Using gas chromatography (GC), the conversion and selectivity of the reduction reaction under the dark and light irradiation conditions can be monitored, demonstrating the enhanced catalytic performance and control over selectivity under LSPR excitation after alloying

non-plasmonic Pd with plasmonic metal Ag. This technique can be adapted to a wide range of molecular transformations and NPs compositions, making it useful for the characterization of the plasmonic catalytic activity of different types of catalysis in terms of conversion and selectivity.

INTRODUCTION:

Among the several applications of metal nanoparticles (NPs), catalysis deserves special attention. Catalysis plays a central role in a sustainable future, contributing to less energy consumption, better utilization of raw materials, and enabling cleaner reaction conditions[1–4]. Thus, progress in catalysis can provide tools for enhancing the atomic efficiency of chemical processes, making them cleaner, more economically viable, and more environmentally friendly. Metal NPs encompassing silver (Ag), gold (Au) or copper (Cu) can display interesting optical properties in the visible range that arise from the unique way these systems interact with light at the nanoscale via the localized surface plasmon resonance (LSPR) excitation[5–8]. In these NPs, referred to as plasmonic NPs, the LSPR comprises the resonant interaction between the incident photons (from an incoming electromagnetic wave) with the collective motion of electrons[5–8]. This phenomenon takes place at a characteristic frequency which is dependent on the size, shape, composition, and dielectric constant of the environment [9–11]. For example, for Ag, Au, and Cu, these frequencies can range from the visible to the near-IR, opening up possibilities for the utilization of solar energy to excite their LSPR[5–8, 12, 13].

Recently, it has been demonstrated that the LSPR excitation in plasmonic NPs can contribute to accelerate the rates and control the selectivity of molecular transformations[5,14–19]. This gave birth to a field called plasmonic catalysis, which focus on using energy from light to accelerate, drive, and/or control chemical transformations[5,14–19]. In this context, it has been established that the LSPR excitation in plasmonic NPs can lead to the formation of energetic hot electrons and holes, referred to as LSPR-excited hot carriers. These carriers can interact with adsorbed species through electronic or vibrational activation[15,16]. In addition to increased reaction rates, this process can also provide alternative reaction pathways not accessible via traditional thermochemically-driven processes, opening up new avenues for the control over reaction selectivity[20–25]. Importantly, it is worth noting that the plasmon decay can also lead to thermal dissipation, leading to a temperature increase in the vicinity of the NPs which can also contribute to speed up reaction rates[15,16].

Due to these interesting features, plasmonic catalysis has been successfully employed towards a variety of molecular transformations[18]. Nevertheless, an important challenge remains. While plasmonic NPs such as Ag and Au display excellent optical properties in the visible and near-IR ranges, their catalytic properties are limited in terms of the scope of transformations. In other words, they do not display good catalytic properties for several of transformations. Additionally, metals that are important in catalysis, such as palladium (Pd) and platinum (Pt), do not support LSPR excitation in the visible or near-IR ranges. To bridge this gap, bimetallic NPs containing a plasmonic and catalytic metal represents an effective strategy[20,26–29]. In these systems, the plasmonic metal can be employed as an antenna to harvest energy from the light excitation through the LSPR, which is then used to drive, accelerate, and control molecular transformations at the catalytic metal. Therefore, this strategy enables us to extend plasmonic catalysis beyond

traditional plasmonic metal NPs[20, 26–29].

This protocol describes the facile synthesis of bimetallic silver-palladium (Ag-Pd) alloyed NPs supported on ZrO_2 (Ag-Pd/ZrO_2) that can act as a plasmonic-catalytic system for plasmonic catalysis. The Ag-Pd/ZrO_2 NPs were prepared by co-impregnation of the corresponding metal precursors on the ZrO_2 support followed by simultaneous reduction[30]. This approach led to the formation of bimetallic NPs around 10 nm in size (diameter) directly at the surface of the ZrO_2 support. The NPs were composed of 1 mol% of Pd to minimize the utilization of the catalytic metal while maximizing the optical properties of the resulting Ag-Pd NPs. A protocol for the application of the Ag-Pd/ZrO_2 NPs in plasmonic catalysis was demonstrated for the reduction of nitrobenzene. We employed 425 nm LED illumination for the LSPR excitation. Gas chromatography was performed to monitor the conversion and selectivity of the reduction reaction under the dark and light irradiation conditions. LSPR excitation led to enhanced catalytic performance and control over selectivity in Ag-Pd/ZrO_2 NPs relative to purely thermally driven conditions. The method described in this protocol is based on a simple photocatalytic reaction setup coupled with gas chromatography and can be adapted to a wide range of molecular transformations and NPs compositions. Thus, this method makes possible the characterization of photocatalytic activity, in terms of conversion and reaction selectivity, of different NPs and for a myriad of liquid-phase transformations. We believe this article will provide important guidelines and insights to both newcomers and more experienced scientists in the field.

PROTOCOL:

1. Synthesis of Ag-Pd/ZrO_2 NPs

NOTE: In this procedure, the Pd mol% in Ag-Pd corresponded to 1%, and the Ag-Pd loading on ZrO_2 corresponded to 3 wt.%.

1.1. Place 1 g of ZrO_2 powder in a 250 mL beaker.

1.2. Add 50 mL of an $AgNO_3$ (aq) (0.0059 mol/L) and 9.71 mL of a K_2PdCl_4 (aq) (0.00031 mol/L) solutions to the beaker under vigorous magnetic stirring (500 rpm) at room temperature.

1.3. Add 10 mL of lysine (0.53 M) aqueous solution.

1.4. Keep the mixture under vigorous stirring (500 rpm) for 20 min.

1.5. After 20 min, use a pipette to add to the suspension 10 mL of a freshly prepared $NaBH_4$ (aq) (0.035 M) solution dropwise, at a rate of 1 mL/min. Keep the suspension under stirring (500 rpm) throughout the process.

1.6. Let the mixture stir for 30 min at room temperature.

2. Separation and purification of the catalyst

2.1. Transfer the suspension to centrifuge tubes and separate the solids from the mixture by centrifugation at 3,260 *x g* for 10 min.

2.2. Carefully remove the liquid phase with a pipette and add 15 mL deionized water to the tubes.

2.2.1. Shake vigorously until dispersion of the solid is obtained. If good dispersion is not achieved, place the tubes in an ultrasonic bath for 5 min.

2.2.2. Centrifuge the dispersion at 3,260 *x g* for 10 min.

2.3. Repeat the washing steps (2.2. to 2.2.2.) two more times using deionized water, then once using ethanol instead of water.

2.4. Remove the ethanol and dry the solid in an oven at 60 °C for 24 h.

2.5. Characterize the prepared Ag-Pd/ZrO_2 NPs by a variety of microscopy, elemental, and spectroscopic techniques.

3. Synthesis of Ag/ZrO_2 NPs

NOTE: In this procedure, Ag loading on ZrO_2 corresponded to 3 wt.%.

3.1. Place 1 g of ZrO_2 powder in a 250 mL beaker.

3.2. Add 50 mL of an $AgNO_3$ (aq) (0.0059 mol/L) solution to the beaker under vigorous magnetic stirring (500 rpm) at room temperature.

3.3. Add 10 mL of lysine (0.53 M) aqueous solution.

3.4. Keep the mixture under vigorous stirring (500 rpm) for 20 min.

3.5. After 20 min, use a pipette to add to the suspension 10 mL of a freshly prepared $NaBH_4$ (aq) (0.035 M) solution dropwise, at a rate of 1 mL/min. Keep the suspension under stirring (500 rpm) throughout the process.

3.6. Let the mixture stir for 30 min under room temperature.

4. Separation and purification of the catalyst

4.1. Transfer the suspension to centrifuge tubes and separate the solids from the mixture by centrifugation at 3,260 *x g* for 10 min.

4.2. Carefully remove the liquid phase with a pipette and add 15 mL deionized water to the tubes.

4.2.1. Shake vigorously until the dispersion of the solid is observed. If good dispersion is not achieved, place the tubes in an ultrasonic bath for 5 min.

4.2.2. Centrifuge the dispersion at 3,260 *x g* for 10 min.

4.3. Repeat the washing steps (4.2. to 4.2.2.) two more times using deionized water, then once using ethanol instead of water.

4.4. Remove the ethanol and dry the solid in an oven at 60 °C for 24 h.

4.5. The prepared Ag/ZrO_2 NPs can then be characterized by a variety of microscopy, elemental, and spectroscopic techniques.

5. Investigation of plasmonic catalytic performance towards the nitrobenzene reduction under LSPR excitation (light illumination)

5.1. Place 30 mg of catalyst in a 25 mL round-bottom flask along with a magnetic stirring bar.

5.2. Add 5 mL of a solution of nitrobenzene (0.03 mol/L) in isopropyl alcohol (IPA) to the reactor.

5.3. Then, add 11.22 mg of KOH powder (0.0002 mol).

5.4. Purge the reactor by bubbling the suspension with an argon flow for 1 min. Immediately after purging, seal the flask.

5.5. Place the reactor in an oil bath heated at 70 °C above a temperature-controlled magnetic stirrer (500 rpm).

5.6. Irradiate the tube using 4 LED lamps with a wavelength of 425 nm as the light source, and a light intensity of 0.5 W/cm^2. The distance from the lamps to the reaction flask should be 7 cm.

5.7. Let the reaction proceed for 2.5 h at 70 °C under vigorous magnetic stirring (500 rpm).

5.8. Then, turn the light off, open the reactor and use a syringe and a needle to collect a 1 mL sample. Filter it through a 0.45 µm filter, to remove the catalyst particulates, into a gas chromatography vial.

6. Reaction in the absence of LSPR excitation (dark conditions)

6.1. Follow the same steps as described in 5, but without light irradiation. Wrap the reaction tube with aluminium foil to prevent any light exposure.

7. Gas chromatography (GC) analysis preparation

7.1. Prepare an IPA solution containing approximately 30 mmol/L nitrobenzene (NB), 30 mmol/L of aniline (AN), and 30 mmol/L of azobenzene (AB).

7.2. Run a GC analysis of the solution using a suitable method. Different methods can be tested by varying the column temperature and gas flow programs. The selected method should be able to separate the peaks corresponding to IPA, NB, AN, and AB in the minimum period of retention time.

7.3. Once the method has been selected, prepare a set of solutions of 50 mM, 25 mM, 10 mM, 5 mM and 2.5 mM NB in IPA, and another set of solutions of AN and AB in IPA with the same concentrations.

7.4. Run a GC analysis of the prepared solutions. Each chromatogram should present 2 peaks: the higher one corresponds to IPA and the lower one corresponds to NB, AN, or AB. For each chromatogram, note down the retention time and peak area of all the peaks.

7.5. Trace the calibration curves of NB, AN, and AB by plotting the concentration versus peak area of each sample.

8. GC analysis

8.1. Run a GC analysis on the samples collected in steps 5. and 6. with the same method used for steps 7.2. and 7.4.

8.2. For each chromatogram, note down the retention time and peak area and use the calibration curves plotted previously to determine the concentration of NB, AN, and AB in the samples.

8.3. Calculate the nitrobenzene conversion as well as the aniline and azobenzene selectivity using the equations:

$$Conversion\ (\%) = \frac{C_{NB}^{0} - C_{NB}}{C_{NB}^{0}} * 100$$

$$AN\ Selectivity\ (\%) = \frac{C_{AN}}{C_{NB}^{0} - C_{NB}} * 100$$

$$AB\ Selectivity\ (\%) = \frac{C_{AB}}{C_{NB}^{0} - C_{NB}} * 100$$

Where C_{NB}^{0} is the initial NB concentration (0.03 mol/L), and C_{NB}, C_{AN}, C_{AB} correspond to the NB, AN, and AB concentrations, respectively, after 2.5 hours reaction by the GC analysis.

REPRESENTATIVE RESULTS:

Figure 1A shows digital photographs of the solid samples containing the pure ZrO_2 oxide (left) and the Ag-Pd/ZrO_2 NPs (right). This change in color from white (in ZrO_2) to brown (Ag-Pd/ZrO_2) provides the initial qualitative evidence on the deposition of Ag-Pd NPs at the ZrO_2 surface. **Figure 1B** shows the UV-visible absorption spectra from the Ag-Pd/ZrO_2 NPs (blue trace) as well as ZrO_2 (black trace) and Ag/ZrO_2 NPs (red trace). Here, the ZrO_2 support and Ag/ZrO_2 NPs were employed as reference materials. ZrO_2 did not display any bands in the visible range. Therefore, it should not contribute to any photocatalytic activity. A signal centered at 428 nm could be detected for the Ag/ZrO_2 NPs (red trace). This signal is assigned to the LSPR dipolar mode in Ag NPs[9]. The Ag-Pd/ZrO_2 NPs displayed a peak centered at 413 nm which is slightly blue-shifted and lower in intensity relative to the Ag/ZrO_2 NPs. The blue shift could be assigned to the change in material permittivity upon alloying with Pd[31]. Also, the decrease in the peak intensity is evidence on the formation of alloyed Ag-Pd NPs, as it is well established that the addition of a non-plasmonic metal to a plasmonic nanoparticle leading to core-shell or alloyed systems lead to the damping in the intensity of the LSPR peak[32]. It is important to note that in this case, we kept the Pd wt. % in the Ag-Pd NPs low (~1 %) so that the LSPR peak is not completely suppressed and the Ag-Pd samples still retain optical properties (LSPR excitation) in the visible range and therefore are active for plasmonic catalysis.

[Place **Figure 1** here]

During the synthesis of the catalysts, the amount of Ag and Pd salt used were calculated in order to reach 3 wt. % metal loading on the support, and a composition of 99% Ag and 1% Pd by weight (wt.%) for Ag-Pd/ZrO_2. To verify the composition of the catalysts, an Atomic Emission Spectroscopy (AES) study was conducted. Calculated amounts of Ag/ZrO_2 and Ag-Pd/ZrO_2 were digested in concentrated nitric acid. The obtained solutions were then analyzed by AES and the amount of Ag initially present in the catalysts was deduced from calibration curves. To determine the Pd content of Ag-Pd/ZrO_2, the same process was employed, except that the catalyst was digested using *aqua regia*. The AES results revealed that the metal loading was 2.6 wt.% for both catalysts, while the composition of the Ag-Pd was 1 wt.% Pd as expected.

Figures 2 show scanning (SEM, **Figure 2A**) and transmission electron microscopy (TEM, **Figure 2B**) of the Ag-Pd/ZrO_2 NPs. The Ag-Pd NPs at the surface of the ZrO_2 supports are difficult to be identified from SEM images (**Figure 2A**) due to their small NPs sizes. However, the formation of Ag-Pd NPs with mean particle size around 10 nm (**Figure 2C**) in diameter can be identified from the TEM images (some of them are indicated by the arrows in **Figure 2B** for clarity). They displayed a spherical shape and a relatively uniform dispersion over the surface of the ZrO_2 supports.

[Place **Figure 2** here]

After the synthesis of Ag-Pd NPs supported on ZrO_2, this method focused on the application as alloyed systems in plasmonic catalysis. Specifically, it describes the utilization of the reduction of nitrobenzene as a model transformation in the liquid phase as illustrated in **Figure 3**. This probe reaction is interesting as the reduction of nitrobenzene can lead to the formation of azobenzene

and aniline[33,34]. Therefore, this model transformation enables the simultaneous investigation of conversion percentages and reaction selectivity as a function of the light illumination (LSPR excitation) in plasmonic catalysis. Here, the reaction was performed in the presence of isopropanol as the solvent and KOH. Also, 70 ^{o}C was employed as the reaction temperature, four 425 nm LED lamps were employed as the light illumination source, and 2.5 h was the reaction time (as described in section 5 of the protocol). In addition to the use of Ag-Pd/ZrO_2 NPs as plasmonic catalysts, blank reactions (absence of catalyst), and Ag/ZrO_2 NPs as reference catalysts to demonstrate the role of Pd in the alloyed bimetallic NPs were also described.

[Place **Figure 3** here]

Figures 4 show a scheme (**Figure 4A**) and a digital photograph (**Figure 4B**) of the reactor and lamps setup employed in the plasmonic catalysis investigation. The setup used for LSPR excitation was made of four 425 nm LED lamps equally spaced around the reactor, at a distance of 7 cm. The reactor was positioned in the center of the system, immersed in an oil bath over a temperature-controlled magnetic stirrer. This enables control over the temperature and more uniform illumination of the reaction mixture from all directions.

[Place **Figure 4** here]

After the reaction proceeds, the conversion and selectivity for the formation of azobenzene and aniline can be measured by gas chromatography. **Figures 5** show the chromatograms obtained at the end of the reaction catalyzed by Ag-Pd/ZrO_2 NPs that was carried out under LSPR excitation (**Figure 5A**) and dark conditions (**Figure 5B**). In this case, one must ensure to use a GC method that enables the separation of nitrobenzene, azobenzene, and aniline in different retention times to correctly identify these molecules, while calibration curves for each molecule were employed to perform their quantification. Moreover, the reaction mixture can also be analyzed by gas chromatography-mass spectrometry (GC-MS) to confirm the formation of azobenzene and aniline and also for any other products that could be formed.

[Place **Figure 5** here]

Table 1 and **Figures 6** depict the conversion percentages for the nitrobenzene reduction (**Figure 6A**) and the selectivity towards azobenzene and aniline (**Figure 6B**) under light illumination for the alloyed Ag-Pd/ZrO_2 NPs as well as for Ag/ZrO_2 NPs. In the absence of any catalysts (blank reactions), no nitrobenzene conversion was detected both in the presence and absence of light illumination. For Ag/ZrO_2 NPs, while no conversion was detected in the dark, a 36% conversion was observed under LSPR excitation. A 56% selectivity towards azobenzene (18% selectivity towards aniline) was detected. This result indicates that the Ag alone can catalyze this reaction under LSPR excitation. For the bimetallic Ag-Pd/ZrO_2 NPs, no significant conversion was detected under dark conditions (2.2%). Interestingly, under LSPR excitation, the conversion % corresponded to 63%, with a 73% selectivity towards azobenzene (27% selectivity towards aniline). This observation demonstrates the potential of the bimetallic configuration in plasmonic-catalytic nanoparticles not only to increase conversion under LSPR excitation but also

to control reaction selectivity.

[Place **Table 1** here]

[Place **Figure 6** here]

FIGURE AND TABLE LEGENDS:

Figure 1: Optical characterization of the catalysts. (**A**) Digital photography of the solid ZrO_2 supports (left) and Ag-Pd/ZrO_2 catalyst (right). (**B**) UV-Visible extinction spectra of ZrO_2, Ag/ZrO_2, and Ag-Pd/ZrO_2 catalysts. The spectra were recorded using an integration sphere in Diffuse Reflectance Spectra (DRS) mode.

Figure 2: Morphological analysis of the Ag-Pd/ZrO_2 catalyst. (**A**) SEM image of the Ag-Pd/ZrO_2 catalyst. (**B**) TEM image of the Ag-Pd/ZrO_2 catalyst. The white arrows depict examples of regions containing Ag-Pd NPs. (**C**) Histogram of the size distribution of Ag-Pd NPs on the Ag-Pd/ZrO_2 catalyst.

Figure 3: Schematic representation of the model reaction. Scheme of the photocatalyzed nitrobenzene reduction used as model reaction. Under LSPR excitation, this reaction leads to the formation of azobenzene and aniline as products.

Figure 4: Representation of the photocatalytic reaction set-up. (**A**) Top-view scheme and (**B**) digital photography of the light reaction setup including the reactor in an oil bath surrounded by four 425 nm LED lamps positioned at 7 cm distance from the reactor.

Figure 5: Chromatograms of the reaction mixture. GC chromatograms obtained from the reaction mixture after 2.5 h catalysis by Ag-Pd/ZrO_2 under LSPR excitation (light irradiation) (**A**) and dark (**B**) conditions.

Table 1: Summary of the conversion and selectivity for the nitrobenzene reduction. Conversion and product selectivity for nitrobenzene reduction reaction under LSPR excitation and dark conditions. Peaks were not detected (ND) if their area was less than 10 000 counts. Ag-Pd/ZrO_2 and Ag/ZrO_2 were employed as catalysts and a blank reaction without any catalyst was also analyzed. Reaction conditions: catalyst (30 mg), solvent (IPA, 5 mL), base (KOH, 0.2 mmol/L) and reactant (nitrobenzene, 0.15 mmol/L), under Ar atmosphere, 2.5 h at 70 ˚C.

Figure 6: Conversion percentage and selectivity under light illumination. (**A**) Nitrobenzene conversion under 425 nm light irradiation and in the dark for the reaction catalyzed by Ag-Pd/ZrO_2 (blue bar) and Ag/ZrO_2 (red bar). (**B**) Aniline and azobenzene selectivity under light irradiation for the reaction catalyzed by Ag-Pd/ZrO_2 (blue bars) and Ag/ZrO_2 (red bars).

DISCUSSION:

The findings described in this method demonstrate that the intrinsic catalytic activity of Pd (or

other catalytic but not plasmonic metal) can be significantly enhanced by LSPR excitation via visible-light irradiation in bimetallic alloyed NPs[35]. In this case, Ag (or another plasmonic metal) is capable of harvesting energy from visible-light irradiation via LSPR excitation. The LSPR excitation leads to the formation of hot charge carriers (hot electrons and holes) and localized heating[5,14–19]. While localized heating can contribute to enhanced reaction rates, the LSPR-excited charge carriers can participate in the vibrational or electronic activation of surface adsorbates[5, 14–19]. This allows for not only increased reaction rates but also changes in reaction selectivity due to selective activation of adsorbates or molecular orbitals at the metal-molecule interface, for example[20–25]. The method described herein effectively allows for the merging of plasmonic and catalytic properties in alloyed nanoparticle systems to extend the applicability of plasmonic catalysis to metals that are important in catalysis but do not support LSPR excitation in the visible range. Although the method described here focused on Ag and Pd as the plasmonic and catalytic metals, it can also be applied and adapted to other plasmonic catalytic combinations such as (Ag-Pt, Au-Pd, Au-Pt, etc.). Moreover, the plasmonic and catalytic properties of the bimetallic alloyed NPs can be further tuned by varying the relative molar ratios of the plasmonic and catalytic components. For instance, increasing the amount of Pd would make the nanoparticles more catalytic, while an increase in the Ag content leads to an increase in the optical properties. The synthesis method can also be adapted to achieve core-shell systems via the sequential deposition and reduction of precursors, for example[36]. It is noteworthy that there is also the possibility to extend the scope on the choice of plasmonic components to earth-abundant materials that can also be employed as supports. Examples include metal nitrides (TiN and ZrN) and some oxides (MoO_3) which support LSPR excitation in the visible and near-IR ranges[37–40].

In addition to the scope of the catalytic materials, the method presented in this paper can be applied to several types of liquid phase transformations that include other reductions, oxidations, and coupling reactions, for example[18]. Another advantage of this method is that the lamp's wavelength and number can be changed, which makes possible the study of the impact of the light's intensity and wavelength on the photocatalytic reaction. Wavelength-dependent photocatalytic reactions have been used to correlate the plasmonic properties of photocatalysts to their performance[5, 14–19]. It has been established increased plasmonic catalytic performances are observed when the light wavelength has a better matching to the LSPR extinction position[5, 14–19].

Finally, to be sure that the results are correct and representative, it is important to pay attention to some crucial steps of the protocol. When synthesizing the NPs, the amount of metal precursors added in the reactor must be precisely known. Indeed, a small error on the Pd content, which is exceptionally low, can result in a dramatic change in the catalytic properties. After the synthesis, the drying temperature should not exceed 60 °C, as it would result in possible oxidation of the silver or aggregation of the NPs, once again interfering with the catalytic activity. The atmosphere of the photocatalytic reaction should also be controlled with great care. In our case, if the reactor is opened, the presence of an ambient atmosphere will put an end to the reaction. Thus, if these issues are well controlled, the method presented here can be used to study the plasmonic catalytic activity and selectivity of various plasmonic catalysts toward a wide range of chemical

reactions. This can enable a better understanding of plasmonic catalysis and aid to the design of catalytic systems having target activities and selectivity for a reaction of interest under mild and environmentally friendly conditions.

ACKNOWLEDGMENTS:

This work was supported by the University of Helsinki and the Jane and Aatos Erkko Foundation. S.H. thanks Erasmus+ EU funds for the fellowship.

DISCLOSURES:

The authors have nothing to disclose.

REFERENCES:

1. Dunn, P. J., Hii, K. K. (MIMI), Krische, M. J., Williams, M. T. *Sustainable Catalysis: Challenges and Pratices for the Pharmaceutical and Fine Chemical Industries*. Wiley-Blackwell. (2013).
2. Tzouras, N. V., Stamatopoulos, I. K., Papastavrou, A. T., Liori, A. A., Vougioukalakis, G.C. Sustainable metal catalysis in C–H activation. *Coordination Chemistry Reviews*. **343**, 25–138 (2017).
3. Polshettiwar, V., Varma, R. S. Green chemistry by nano-catalysis. *Green Chemistry*. **12** (5), 743 (2010).
4. Rodrigues, T. S., da Silva, A. G. M., Camargo, P. H. C. Nanocatalysis by noble metal nanoparticles: controlled synthesis for the optimization and understanding of activities. *Journal of Materials Chemistry A*. **7** (11), 5857–5874 (2019).
5. Linic, S., Christopher, P., Ingram, D. B. Plasmonic-metal nanostructures for efficient conversion of solar to chemical energy. *Nature Materials*. **10** (12), 911–921 (2011).
6. Nam, J. M., Liz-Marzán, L., Halas, N. Chemical Nanoplasmonics: Emerging Interdisciplinary Research Field at Crossroads between Nanoscale Chemistry and Plasmonics. *Accounts of Chemical Research*. **52** (11), 2995–2996 (2019).
7. Brongersma, M. L., Halas, N. J., Nordlander, P. Plasmon-induced hot carrier science and technology. *Nature Nanotechnology*. **10** (1), 25–34 (2015).
8. Smith, J. G., Faucheaux, J. A., Jain, P. K. Plasmon resonances for solar energy harvesting: A mechanistic outlook. *Nano Today*. **10** (1), 67–80 (2015).
9. Hartland, G. V. Optical studies of dynamics in noble metal nanostructures. *Chemical Reviews*. **111** (6), 3858–3887 (2011).
10. Kelly, K. L., Coronado, E., Zhao, L. L., Schatz, G. C. The optical properties of metal nanoparticles: The influence of size, shape, and dielectric environment. *Journal of Physical Chemistry B*. **107** (3), 668–677 (2003).
11. Hermoso, W. et al. Triangular metal nanoprisms of Ag, Au, and Cu: Modeling the influence of size, composition, and excitation wavelength on the optical properties. *Chemical Physics*. **423**, 142–150 (2013).
12. Kumar, A. et al. Rational Design and Development of Lanthanide-Doped NaYF4@CdS-Au-RGO as Quaternary Plasmonic Photocatalysts for Harnessing Visible-Near-Infrared Broadband Spectrum. *ACS Applied Materials and Interfaces*. **10** (18), 15565–15581 (2018).

13. Reddy, K. L., Kumar, S., Kumar, A., Krishnan, V. Wide spectrum photocatalytic activity in lanthanide-doped upconversion nanophosphors coated with porous TiO2 and Ag-Cu bimetallic nanoparticles. *Journal of Hazardous Materials*. **367**, 694–705 (2019).
14. Ingram, D. B., Linic, S. Water splitting on composite plasmonic-metal/semiconductor photoelectrodes: Evidence for selective plasmon-induced formation of charge carriers near the semiconductor surface. *Journal of the American Chemical Society*. **133** (14), 5202–5205 (2011).
15. Linic, S., Aslam, U., Boerigter, C., Morabito, M. Photochemical transformations on plasmonic metal nanoparticles. *Nature Materials*. **14** (6), 567–576 (2015).
16. Aslam, U., Rao, V. G., Chavez, S., Linic, S. Catalytic conversion of solar to chemical energy on plasmonic metal nanostructures. *Nature Catalyst.* **1**, 656–665 (2018).
17. Araujo, T. P., Quiroz, J., Barbosa, E. C. M., Camargo, P. H. C. Understanding plasmonic catalysis with controlled nanomaterials based on catalytic and plasmonic metals. *Current Opinion in Colloid and Interface Science*. **39**, 110–122 (2019).
18. Gellé, A. et al. Applications of plasmon-enhanced nanocatalysis to organic transformations. *Chemical Reviews*. 986–1041 (2020).
19. Shaik, F., Peer, I., Jain, P. K., Amirav, L. Plasmon-Enhanced Multicarrier Photocatalysis. *Nano Letters*. **18** (7), 4370–4376 (2018).
20. Quiroz, J. et al. Controlling Reaction Selectivity over Hybrid Plasmonic Nanocatalysts. *Nano Letters.* **18**, 7289–7297 (2018).
21. Peiris, E. et al. Plasmonic Switching of the Reaction Pathway: Visible-Light Irradiation Varies the Reactant Concentration at the Solid–Solution Interface of a Gold–Cobalt Catalyst. *Angewandte Chemie - International Edition*. **58** (35), 12032–12036 (2019).
22. Yu, S., Wilson, A. J., Heo, J., Jain, P. K. Plasmonic Control of Multi-Electron Transfer and C-C Coupling in Visible-Light-Driven CO2 Reduction on Au Nanoparticles. *Nano Letters*. **18** (4), 2189–2194 (2018).
23. Yu, S., Jain, P. K. Plasmonic photosynthesis of C 1 –C 3 hydrocarbons from carbon dioxide assisted by an ionic liquid. *Nature Communications*. **10**, 2022 (2019).
24. Zhang, X. et al. Product selectivity in plasmonic photocatalysis for carbon dioxide hydrogenation. *Nature Communications*. **8**, 1–9 (2017).
25. Cortés, E. Efficiency and Bond Selectivity in Plasmon-Induced Photochemistry. *Advanced Optical Materials*. **5** (15), 1700191 (2017).
26. de Freitas, I. C. et al. Design-controlled synthesis of IrO 2 sub-monolayers on Au nanoflowers: marrying plasmonic and electrocatalytic properties . *Nanoscale*. 23–27 (2020).
27. Zhang, C. et al. Al-Pd Nanodisk Heterodimers as Antenna-Reactor Photocatalysts. *Nano Letters*. **16** (10), 6677–6682 (2016).
28. Zhou, L. et al. Light-driven methane dry reforming with single atomic site antenna-reactor plasmonic photocatalysts. *Nature Energy*. **5**, 61–70 (2020).
29. Swearer, D. F. et al. Heterometallic antenna−reactor complexes for photocatalysis. *Proceedings of the National Academy of Sciences*. **113** (32), 8916–8920 (2016).
30. Peiris, S., Sarina, S., Han, C., Xiao, Q., Zhu, H.-Y. Silver and palladium alloy nanoparticle catalysts: reductive coupling of nitrobenzene through light irradiation. *Dalton Transactions*. **46** (32), 10665–10672 (2017).
31. Rahm, J. M. et al. A Library of Late Transition Metal Alloy Dielectric Functions for Nanophotonic Applications. *Advanced Functional Materials*. **2002122**, adfm.202002122 (2020).

32. Zhang, C., Chen, B. Q., Li, Z. Y., Xia, Y., Chen, Y. G. Surface Plasmon Resonance in Bimetallic Core-Shell Nanoparticles. *Journal of Physical Chemistry C*. **119** (29), 16836–16845 (2015).
33. Liu, Z., Huang, Y., Xiao, Q., Zhu, H. Selective reduction of nitroaromatics to azoxy compounds on supported Ag-Cu alloy nanoparticles through visible light irradiation. *Green Chemistry*. **18** (3), 817–825 (201AD).
34. Chaiseeda, K., Nishimura, S., Ebitani, K. Gold nanoparticles supported on alumina as a catalyst for surface plasmon-enhanced selective reductions of nitrobenzene. *ACS Omega*. **2** (10), 7066–7070 (2017).
35. Peiris, S. et al. Metal nanoparticle photocatalysts: emerging processes for green organic synthesis. *Catalysis Science and Technology.* **6** (2), 320–338 (2016).
36. García-García, I. et al. Silver-Based Plasmonic Catalysts for Carbon Dioxide Reduction. *ACS Sustainable Chemistry and Engineering*. **8** (4), 1879–1887 (2020).
37. Agrawal, A., Johns, R. W., Milliron, D. J. Control of Localized Surface Plasmon Resonances in Metal Oxide Nanocrystals. *Annual Review of Materials Research*. **47** (1), 1–31 (2017).
38. Lounis, S. D., Runnerstrom, E. L., Llordés, A., Milliron, D. J. Defect chemistry and Plasmon physics of colloidal metal oxide Nanocrystals. *Journal of Physical Chemistry Letters*. **5** (9), 1564–1574 (2014).
39. Rej, S. et al. Determining Plasmonic Hot Electrons and Photothermal Effects during H2 Evolution with TiN–Pt Nanohybrids. *ACS Catalysis*. **10** (9), 5261–5271 (2020).
40. Barragan, A. A. et al. Photochemistry of Plasmonic Titanium Nitride Nanocrystals. *The Journal of Physical Chemistry C*. **123** (35), 21796–21804 (2019).

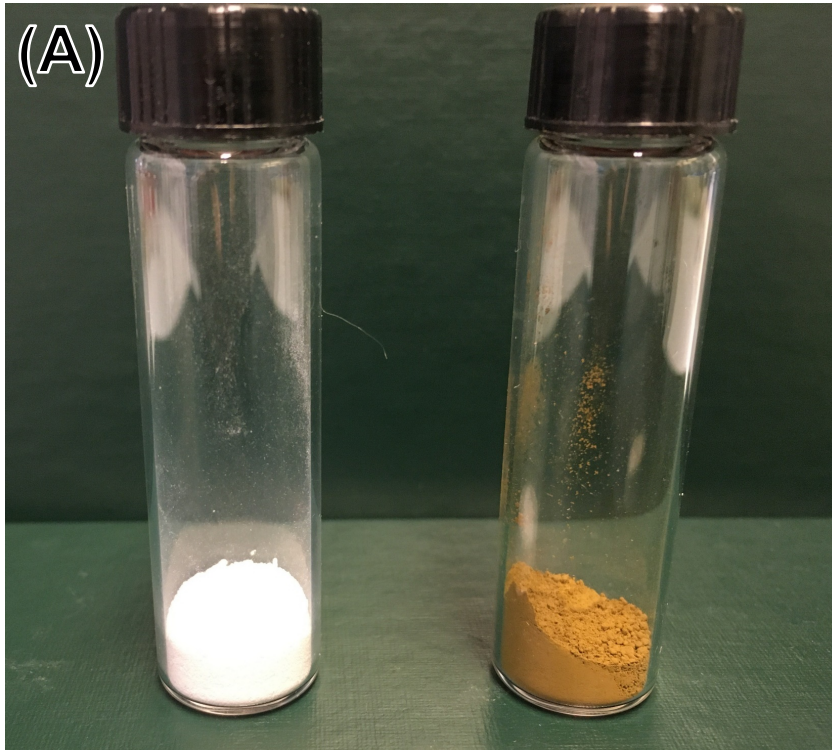
(A)
ZrO2
Ag-Pd/ZrO2

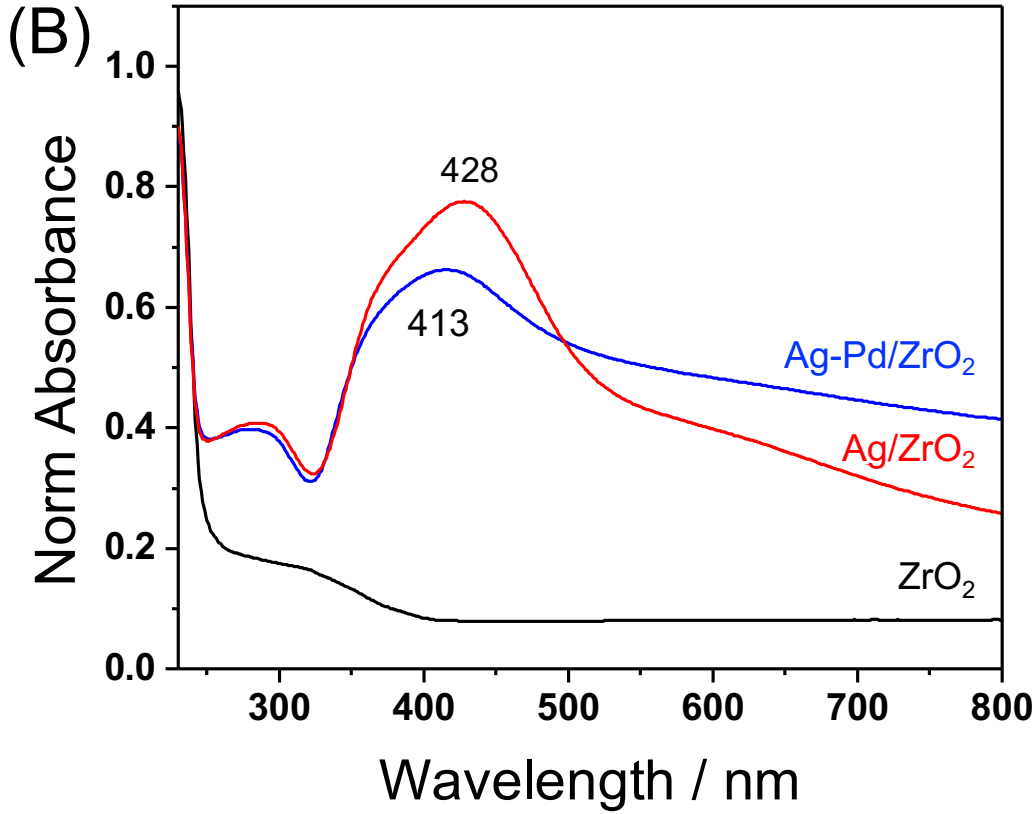
(B)
Norm Absorbance
1.0
0.8
0.6
0.4
0.2
0.0
428
413
Ag-Pd/ZrO2
Ag/ZrO2
ZrO2
300
400
500
600
700
800
Wavelength / nm

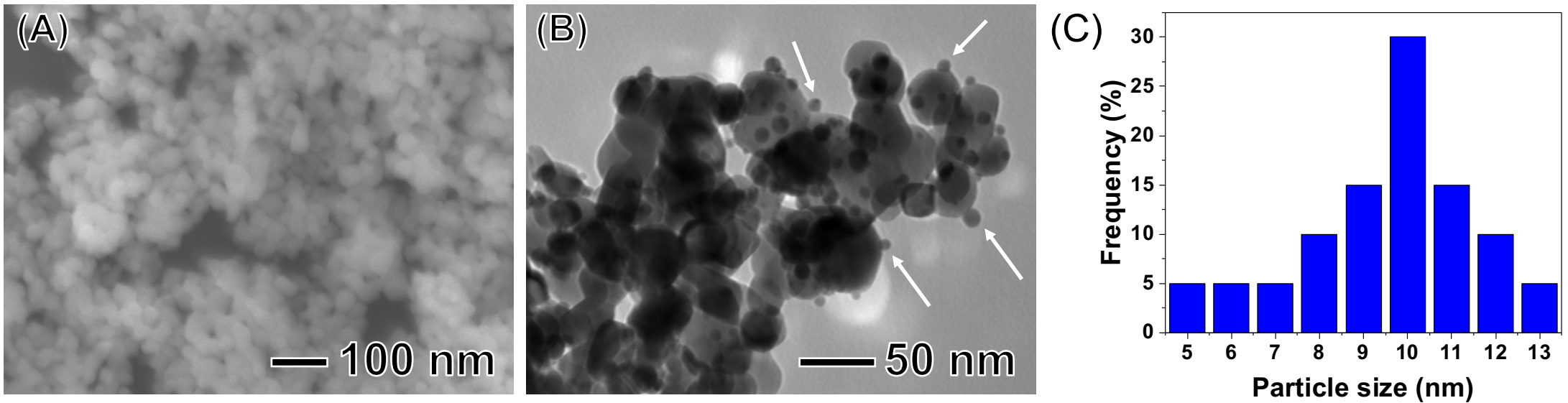
(A)
100 nm
(B)
50 nm
(C)
Frequency (%)
0
5
10
15
20
25
30
5
6
7
8
9
10
11
12
13
Particle size (nm)

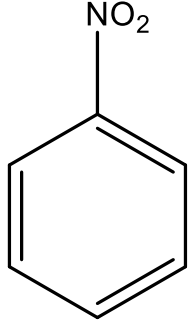

Ag-Pd/ZrO_2 NPs, 2.6 wt %

Pr^{i}OH, KOH, 70 ^{o}C, 2.5 h

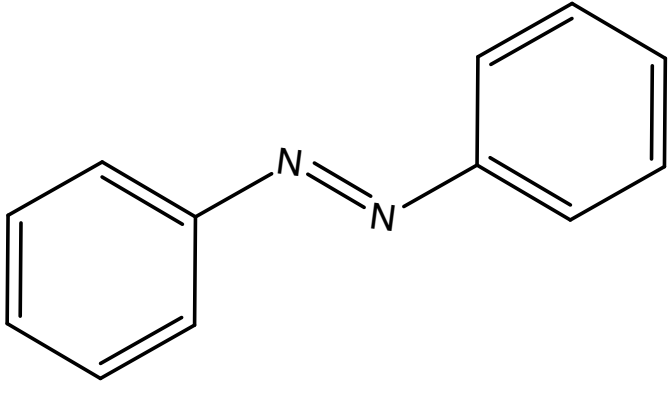

+

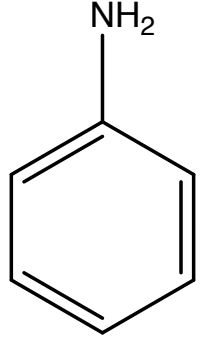

Nitrobenzene

Azobenzene

Aniline

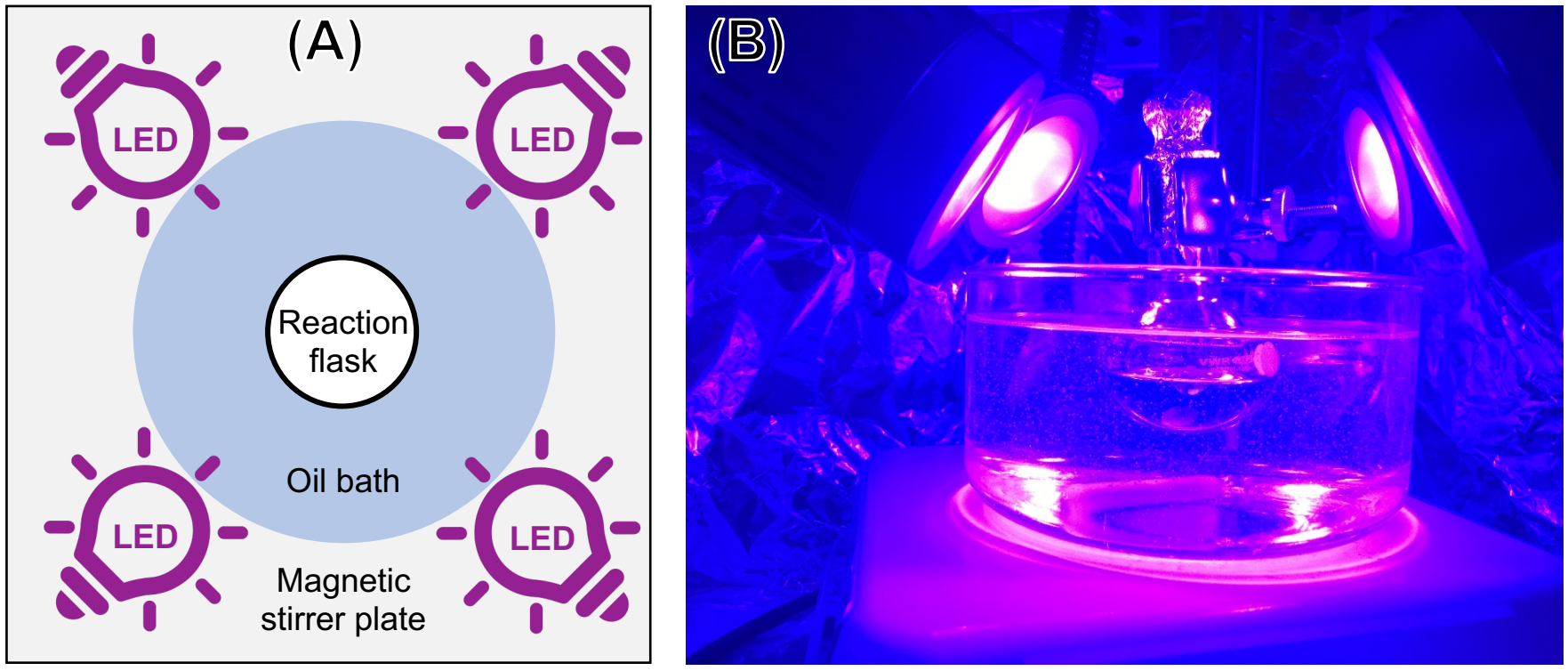
(A)
LED
LED
LED
LED
Reaction flask
Oil bath
Magnetic stirrer plate
(B)

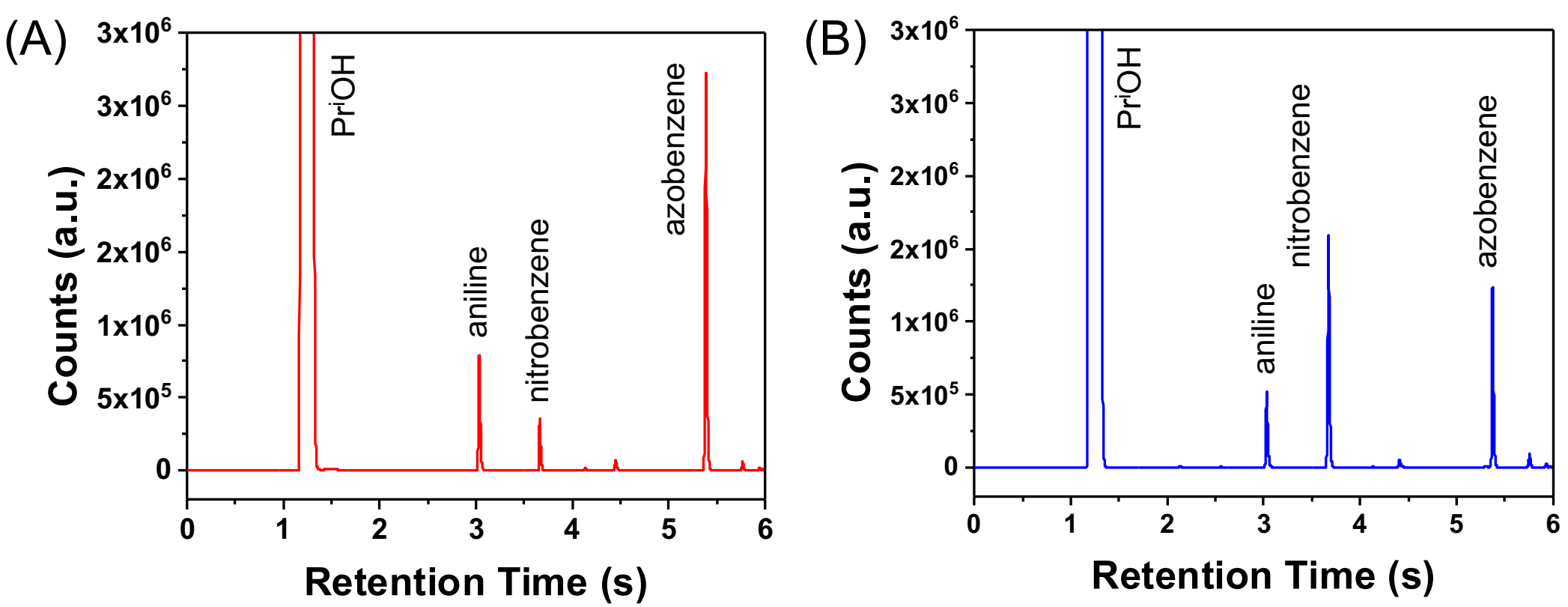
(A)
Counts (a.u.)
3x10^6
3x10^6
2x10^6
2x10^6
1x10^6
5x10^5
0
PriOH
aniline
nitrobenzene
azobenzene
0
1
2
3
4
5
6
Retention Time (s)
(B)
Counts (a.u.)
3x10^6
3x10^6
2x10^6
2x10^6
1x10^6
5x10^5
0
PriOH
aniline
nitrobenzene
azobenzene
0
1
2
3
4
5
6
Retention Time (s)

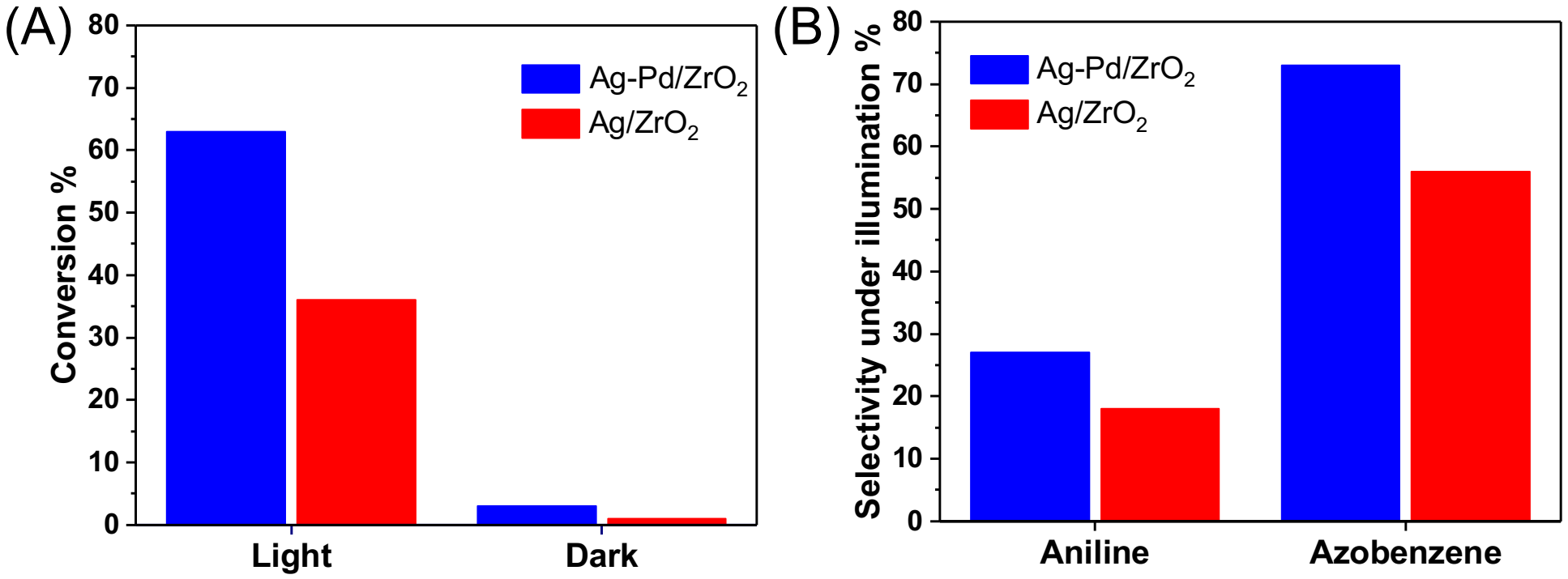
(A)
Conversion %
0
10
20
30
40
50
60
70
80
Ag-Pd/ZrO2
Ag/ZrO2
Light
Dark
(B)
Selectivity under illumination %
0
10
20
30
40
50
60
70
80
Ag-Pd/ZrO2
Ag/ZrO2
Aniline
Azobenzene

Table 1

Catalyst	Condition	Conversion %	
			Aniline
AgPd/ZrO2 (2.56 %)	Light	63	27
	Dark	2.2	ND
Ag/ZrO2 (2.61 %)	Light	36	18
	Dark	0	ND
Blank	Light	0	ND
	Dark	0	ND

Selectivity %
Azobenzene
73
ND
56
ND
ND
ND

Name of Material/Equipment	Company	Catalog Number	CAS Number
2-Propanol (anhydrous, 99.5%)	Sigma-Aldrich	278475	67-63-0
Aniline (for synthesis)	Sigma-Aldrich	8.22256	62-53-3
Azobenzene (98%)	Sigma-Aldrich	424633	103-33-3
Ethanol	Honeywell	32221	64-17-5
Hydrochloric acid (37%)	VWR	PRLSMC310066	7647-01-0
L-Lysine (crystallized, ≥98.0% (NT))	Sigma-Aldrich	62840	56-87-1
Nitric acid (65%)	Merck	100456	7697-37-2
Nitrobenzene	Sigma-Aldrich	8.06770	98-95-3
Potassium hydroxide	Fisher	10448990	1310-58-3
Potassium tetrachloropalladate (II) (98%)	Sigma-Aldrich	205796	10025-98-6
Silver nitrate (ACS reagent, ≥99.0%)	Sigma-Aldrich	209139	7761-88-8
Sodium borohydride (fine granular for synthesis)	Sigma-Aldrich	8.06373	16940-66-2
Zirconium (IV) oxide (nanopowder, <100 nm particle size (TEM))	Sigma-Aldrich	544760	1314-23-4

Comments/Description

UNIVERSITY OF HELSINKI
FACULTY OF SCIENCE

Pedro H. C. Camargo, Ph.D

Professor of Inorganic Materials Chemistry
Department of Chemistry
Faculty of Science

June 30th, 2020

Re: JoVE61712.R1

Dr. Vineeta Bajaj,
Review Editor, JoVE

Dear Vineeta Bajaj,

Thank you for your e-mail dated June 17th, 2020, regarding your decision on our manuscript JoVE61712. We would like to thank the editor and reviewers for their positive appraisal of the manuscript and the changes suggested by the editor and referees were gratefully received. We have addressed all the issues highlighted by the editor and reviewers as shown below. It is hoped that the revised review is now suitable for publication in JoVE. Moreover, we added Kjell Knapas as a co-author in the manuscript as he helped us to perform the AES analyses as required by the reviewers. This is highlighted in yellow on page 1 of our revised ms.

Editorial comments:

Changes to be made by the Author(s):
1. Please take this opportunity to thoroughly proofread the manuscript to ensure that there are no spelling or grammar issues. The JoVE editor will not copy-edit your manuscript and any errors in the submitted revision may be present in the published version.
2. Please format the manuscript as: paragraph Indentation: 0 for both left and right and special: none, Line spacings: single. Please include a single line space between each step, substep and note in the protocol section. Please use Calibri 12 points
3. Please rephrase the Short Abstract/Summary to clearly describe the protocol and its applications in complete sentences between 10-50 words: “Presented here is a protocol …”
4. Please define all abbreviations during the first-time use.
5. Unfortunately, there are a few sections of the manuscript that show significant overlap with previously published work. Though there may be a limited number of ways to describe a technique, please use original language throughout the manuscript. Please see lines: 61-63, 63-65, 74-75, 77-80, 82-84.
6. Please ensure the Introduction includes all of the following:

a) A clear statement of the overall goal of this method
b) The rationale behind the development and/or use of this technique
c) The advantages over alternative techniques with applicable references to previous studies
d) A description of the context of the technique in the wider body of literature
e) Information to help readers to determine whether the method is appropriate for their application
7. Please ensure that all text in the protocol section is written in the imperative tense as if telling someone how to do the technique (e.g., “Do this,” “Ensure that,” etc.). The actions should be described in the imperative tense in complete sentences wherever possible. Avoid usage of phrases such as “could be,” “should be,” and “would be” throughout the Protocol. Any text that cannot be written in the imperative tense may be added as a “Note.” However, notes should be concise and used sparingly.
8. The Protocol should contain only action items that direct the reader to do something.
9. Please add more details to your protocol steps. Please ensure you answer the “how” question, i.e., how is the step performed?
10. Please ensure that individual steps of the protocol should only contain 2-3 actions sentences per step.
11. There is a 10-page limit for the Protocol, but there is a 2.75-page limit for filmable content. Please highlight 2.75 pages or less of the Protocol (including headings and spacing) that identifies the essential steps of the protocol for the video, i.e., the steps that should be visualized to tell the most cohesive story of the Protocol.
12. Please describe the result with respect to your experiment, you performed an experiment, how did it help you to conclude what you wanted to and how is it in line with the title.
13. Please remove the embedded figure(s) from the manuscript. All figures should be uploaded separately to your Editorial Manager account. Each figure must be accompanied by a title and a description after the Representative Results of the manuscript text.
14. Please discuss all figures in the Representative Results. However, for figures showing the experimental set-up, please reference them in the Protocol.
15. Each Figure Legend should include a title and a short description of the data presented in the Figure and relevant symbols.
16. Please remove the embedded Table from the manuscript. All tables should be uploaded separately to your Editorial Manager account in the form of an .xls or .xlsx file. Each table must be accompanied by a title and a description after the Representative Results of the manuscript text.
17. Please obtain explicit copyright permission to reuse any figures from a previous publication. Explicit permission can be expressed in the form of a letter from the editor or a link to the editorial policy that allows re-prints. Please upload this information as a .doc or .docx file to your Editorial Manager account. The Figure must be cited appropriately in the Figure Legend, i.e. “This figure has been modified from [citation].”
18. As we are a methods journal, please ensure that the Discussion explicitly cover the following in detail in 3-6 paragraphs with citations:

a) Critical steps within the protocol
b) Any modifications and troubleshooting of the technique
c) Any limitations of the technique
d) The significance with respect to existing methods
e) Any future applications of the technique
19. Please revise the table of the essential supplies, reagents, and equipment. The table should include the name, company, and catalog number of all relevant materials in separate columns in an xls/xlsx file.

All these editorial changes were performed in our revised manuscript as suggested. The pages of the protocol that identifies the essential steps of the protocol for the video are highlighted in green. The highlights in yellow refers to changes and improvements suggested by the reviewers.

Reviewer #1:

This manuscript nicely describe the synthesis of AgPd nanoparticles on a ZrO2 support and their photocatalytic performance towards the selectivity in the nitrobencene reduction reaction. The manuscript is very nicely written, clear and perfectly organized. The information presented here is relevant for a broad audience of chemists and material scientists and it should be accepted for publication in its current format.

Reviewer #2:

Major Concerns:
1. My hypothesis is that these nanoparticles are AgPd alloys rather than the conventional antenna-reactor configuration in which the plasmonic and catalytic metals are spatially separated (refs 25, 27). If they are alloys, I also suggest referring to them as such since it will align better with literature on nanoparticle catalysts.

We agree with the reviewer that the nanoparticles are Ag-Pd alloys. This was clarified in our revised manuscript as highlighted in yellow on pages 01, 03, and 08-10

2. On line 132, there seems to be a typo - I believe the authors mean NaBH4?

This was clarified in our revised manuscript as highlighted in yellow in line 170.

3. In Table 1, the conversion and selectivity percentage for all catalyst/illumination condition combinations should be given unless it was undetectable, in which case there should be an upper bound reported. For example, from Figure 6A, it looks like there is a small but detectable conversion percentage for the dark case for both AgPd and Ag, but this is only reported in the table for AgPd.

We agree with the reviewer's comments. This has been clarified in the revised version of Table 1 and on Table 1 caption.

Minor Concerns:
1. In the synthesis of AgPd/ZrO2 nanoparticles, I suggest defining the rpm for "vigorous magnetic stirring"

This has been clarified in our revised ms as highlighted in yellow on pages 03 and 04.

2. I would like to see more quantitative numbers on the size distribution of these nanoparticles. I suggest showing a histogram of the nanoparticle sizes. Similarly, line 237 suggests that the Ag/ZrO2 nanoparticles are not of the same size or size distribution as the AgPd nanoparticles, and it would be helpful to see proof of that.

Following the reviewer's recommendation, the histogram of size distribution was included as Figure 2C in our revised manuscript. The differences in the size distributions was implied as a reason to explain the changes in the LSPR band position. However, the size distributions should be similar and the blue-shift in LSPR peak may be attributed to the change in material permittivity upon alloying with Pd (see, for example, https://doi.org/10.1002/adfm.202002122). This was clarified in our revised manuscript as highlighted in yellow on page 07.

3. The axes in Figure 5 are hard to read.

We have prepared a revised version of Figure 5 in which the axes are more readable as suggested by the reviewer.

4. For Figure 6B, it should be made clearer (either in the figure or in the caption) that this is selectivity under illumination.

We clarified this issue both in the figure (y-axis) and caption as suggested.

5. It would be helpful to know/verify that the actual composition of these nanoparticles matches that of the salt concentration. This could be done via ICP, Auger electron spectroscopy, EDX, etc. if possible.

The actual composition of the samples were determined by Atomic Emission Spectroscopy (AES). The results show a metal loading of 2.6 wt.% for both Ag-Pd/ZrO_2 and Ag/ZrO_2 NPs, while the Pd content in the Ag-Pd NPs corresponded to 1 wt. %. This has been clarified in our revised ms as highlighted in yellow on page 07.

6. The blue-shift in LSPR peak (lines 233-237) can also be attributed to the change in material permittivity upon alloying with Pd (see Rahm et al. Advanced Functional Materials 2020).

We agree with the reviewer, and this has been clarified as highlighted in yellow on page 07 of our revised manuscript.

7. In line 297-298, note that there is no LSPR excitation when there aren't any Ag or AgPd nanoparticles. Instead, this should be "in the presence and absence of light illumination".

This has been clarified as highlighted in yellow on page 09 of our revised manuscript.

Reviewer #3:

(1) There are minor errors in the manuscript. For example:
Page 3 line 86-87, sentence need to be modified.
Page 7, line 235-236, intensity of AgPd/ZrO2 NPs should be compared with Ag/ZrO2 NPs.
Page 7, line 228, UV-visible should be written.
Page 8, line 272, need to be modified.

These minor errors have been corrected in our revised manuscript as highlighted in yellow in the corresponding pages.

(2) Please cite and discuss the following relevant literature: ACS Appl. Mater. Interfaces 2018, 10, 15565−15581; Applied Sciences, 2020, 10, 50; Journal of Hazardous Materials, 2019, 367, 694-705.

The reference *Applied Sciences, 2020, 10, 50* refers to a paper entitled 'Debonding Detection of Reinforced Concrete (RC) Beam with Near-Surface Mounted (NSM) Pre-stressed Carbon Fiber Reinforced Polymer (CFRP) Plates Using Embedded Piezoceramic Smart Aggregates (SAs)', which is unrelated to this work.

The other two references were added in our revised manuscript as references 12 and 13 as highlighted in yellow on page 12. We did not discuss them in the text as they mainly focus on plasmonic nanoparticles coupled with semiconductors and up-conversion, which is out of the context of our manuscript and we believe it would confuse the readers.

(3) It is better to provide the synthesis procedure of Ag/ZrO2 in Protocol section.

This was clarified as highlighted in yellow on pages 04 and 05 of our revised manuscript.

(4) How the author has come to the conclusion of loading of 3 wt% of metal loading in the nanocomposite? It may be better to provide some evidence.

The loading was determined by AES as highlighted in yellow on page 07 of our revised manuscript.

(5) Please mention the distance between the LED lamps and reaction flask, as this can influence the activity.

This was clarified as highlighted in yellow on pages 05 and 08 of our revised manuscript.